Comparison Criteria and Stability Analysis of Electrodynamic Thrust Bearings

Joachim Van Verdeghem, Virginie Kluyskens, Bruno Dehez

Center for Research in Mechatronics (CEREM), Institute of Mechanics, Materials and Civil Engineering (IMMC), Université catholique de Louvain (UCL), Louvain-la-Neuve 1348, Belgium, joachim.vanverdeghem@uclouvain.be

***Abstract*— Electrodynamic bearings can ensure contactless levitation of rotors at room temperature solely relying on passive phenomena. Recently, two models describing the axial quasi-static and dynamic behaviours of a wide variety of electrodynamic thrust bearings (EDTBs) have been derived. However, although these models enable to study EDTB topologies in terms of stiffness and rotational losses, criteria allowing us to objectively compare their intrinsic qualities still lack. The present paper thus introduces four comparison criteria related to the axial stiffness, the bearing energy efficiency and the external damping required to stabilise the thrust bearing regardless of the spin speed. To this end, an analytical stability analysis is first performed on the basis of these dynamic models. This notably leads to static and dynamic conditions that ensure the stability at a specific speed. Finally, three topologies are compared on the basis of the comparison criteria in the framework of a case study.**

I. INTRODUCTION

Nowadays, magnetic bearings constitute a convincing alternative to classical solutions such as ball or journal bearings by ensuring contactless guiding of rotors, thereby reducing losses and removing mechanical wear and friction. These compelling bearing can be either active or passive. The former are based on current-controlled electromagnets exerting an attractive force on a ferromagnetic rotor whereas the latter only rely on passive phenomena.

Electrodynamic bearings (EDBs) belong to passive magnetic bearings (PMBs) as they lean on electromagnetic forces generated by the appearance of induced currents conductors in relative motion with respect to a magnetic field produced by permanent magnets (PMs). Although their stiffness is quite low in comparison with active magnetic bearings (AMBs), these bearings are attractive as they do not require sensors, controllers, nor power electronics, thereby being intrinsically more reliable, compact and energy-efficient [1]. EDBs can be of two types: radial or axial bearings. The former allows to guide the radial degrees of freedom of the rotor whereas the latter provides the axial levitation.

Numerous models describing radial EDBs in quasi-static conditions [2][3], i.e. assuming constant spin speed and eccentricity, as well as in dynamic conditions were developed [4][5]. Although they have never been defined as such, several criteria allowing us to compare these EDBs came up along with these models.

Obviously, the stiffness induced by the electrodynamic effects is of primary interest given that it is directly related to the stability and eccentricity. This stiffness is an increasing function of the rotor spin speed and can be characterised through two coefficients, namely the maximal stiffness and the electrical pole of the R/L_c equivalent circuit [6]. Several sensitivity analyses were performed on these coefficients, thus yielding a first insight of the geometrical [7], electrical [8] and magnetic parameters [9] that strongly influence them.

In addition to the stiffness, attention was paid to the rotational losses required to provide the levitation force. Indeed, these losses are dissipated as heat and should therefore be limited to avoid significant temperature rises as well as to increase the energy efficiency. To this end, the null-flux concept was transposed to heteropolar EDBs, allowing us to conceive new topologies whose flux linkage is null when there is no rotor eccentricity [10]. In this way, there is no induced currents and therefore no losses in this position. Similarly, the null-E concept was then developed for homopolar bearings [11]. Simultaneously, analytical formulas were derived to evaluate these rotational losses [12][13].

The dynamic behaviour of radial EDBs constitutes a major issue as these bearings are always unstable in the absence of non-rotating damping, i.e. damping that does not depend on the rotor rotation [5][14]. Considering the difficulty of adding damping in a contactless way, thus being consistent with the magnetic bearing approach, this external damping should be minimised. To this end, analytical expressions were developed on the basis of quasi-static models to determine the minimal damping required to ensure the stability at a particular spin speed [2][9][15].

Despite their promising stability properties, electrodynamic thrust bearings (EDTBs) have focused much less research efforts. A bearing energy efficiency, defined as the ratio between the electrodynamic levitation force and the corresponding power losses, has been introduced as a comparison criterion even though the external forces such as the detent ones can not be taken into account [16]. Recently, two models describing each both the axial quasi-static and dynamic behaviours of EDTBs have been derived, allowing us to study their stiffness and rotational losses [17][18]. By contrast, although the beneficial effect of the external damping has been demonstrated, there is still no formula allowing us to determine the additional damping required to ensure the stability. Similarly, the spin speed ranges within which the EDTB is stable can still not be determined analytically.

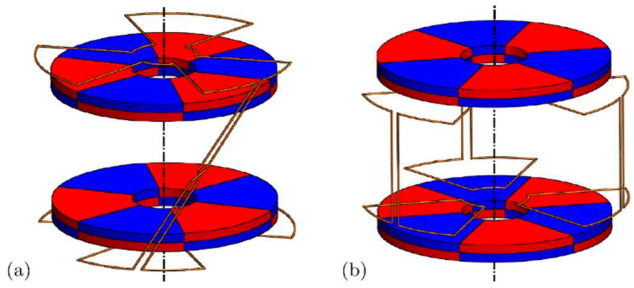

Figure 1. Bearing topologies with only one phase represented. (a) PMs are internal and the p coils of each set are connected in series, the two resulting sets being connected together in series. (b) PMs are external and the p upper and the p lower coils are independently connected together in opposition.

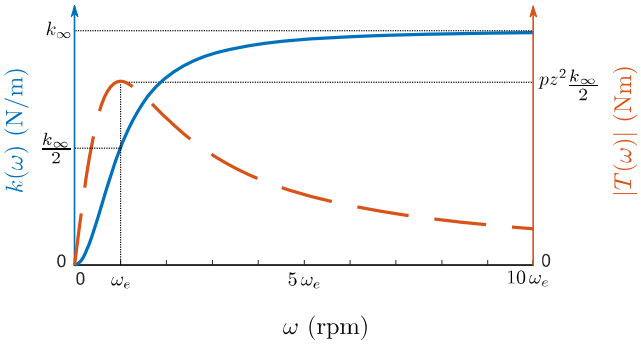

Figure 2. Evolution of the electrodynamic stiffness k (solid line) and braking torque T (dashed line) with the spin speed ω.

In this context, the present paper introduces four comparison criteria related to the axial stiffness, the energy efficiency and the stability, allowing us to compare objectively EDTB topologies in terms of their intrinsic qualities. Analytical expressions of these criteria are derived on the basis of the dynamical models proposed in [17]-[19], thus being suitable for a wide variety of thrust bearings. In addition, static and dynamic stabilities are analysed analytically, providing conditions that ensure that the EDTB is stable at a particular spin speed.

The paper is structured as follows. Section II depicts the thrust bearing topologies under study. Following on from this, the electromechanical model, comprising the electromagnetic and the rotor mechanical models, is described. The stability of the system is then analysed in sections IV. Section V defines the four comparison criteria for EDTBs. The last section is devoted to a case study analysing three topologies through these comparison criteria.

II. Bearing Description

The thrust bearing being analysed is constituted of two independent subassemblies, namely the PM arrangements and the armature winding, in rotary motion relative to each other, as illustrated in Fig. 1. Each of them can be attached either to the stator or to the rotor.

The first subassembly comprises two PM arrangements, each producing an identical axial magnetic field with p pole pairs. These arrangements can:

- either be placed in repulsive or attractive mode, as represented in Fig 1;
- either constitute the internal or external subassembly, as shown in Figs 1(a) and 1(b) respectively.

The armature winding comprises N identical and evenly distributed phase windings. The latter are each constituted of two identical sets of N identical and evenly distributed coils, each set being predominantly magnetically linked to one PM arrangement, and can be of two types:

- the p coils of each set are connected in series, the two resulting sets being connected together, as illustrated in Fig. 1(a);
- the p upper and the p lower coils are independently connected together, as represented in Fig. 1(b).

Besides, as illustrated in Figs. 1(a) and 1(b) respectively, both upper and lower sets of coils can be shifted by an angle equal to π/p or zero and can be either connected in series or in opposition. This connection is chosen on the basis of the angular shift that separates the upper and lower sets as well as the attractive or repulsive mode of the PM arrangements so as to ensure that the flux linked by the armature winding is null when the rotor is axially centered with respect to the stator, thereby respecting the null-flux principle.

III. Electromechanical Model

Under the assumption of small rotor axial, radial and angular displacements and neglecting the inductance coefficient variations with these displacements, the axial dynamics of the system constituted of the rotor and the ETDB is decoupled from the radial and angular ones [20]. Assuming in addition that the rotor spin speed varies slowly compared to the axial dynamics, the latter can be described through a linear state-space representation as extensively derived in [17]:

$$\begin{bmatrix} \ddot{z} \\ \dot{z} \\ \dot{F} \\ \dot{T/z} \end{bmatrix} = \mathbf{A} \begin{bmatrix} \dot{z} \\ z \\ F \\ T/z \end{bmatrix} + \frac{F_e}{M} \begin{bmatrix} 1 \\ 0 \\ 0 \\ 0 \end{bmatrix}, \tag{1}$$

with:

$$\mathbf{A} = \begin{pmatrix} -\frac{C}{M} & -\frac{k_e}{M} & \frac{1}{M} & 0 \\ 1 & 0 & 0 & 0 \\ -\frac{K_\Phi^2\, N}{2L_c} & 0 & -\frac{R}{L_c} & \omega \\ 0 & -\omega p^2 \frac{K_\Phi^2\, N}{2L_c} & -\omega p^2 & -\frac{R}{L_c} \end{pmatrix}, \tag{2}$$

where z and $\dot{z}$ are respectively the axial position and velocity, F and T are respectively the electrodynamic force and braking torque, F_e is the axial external force acting on the rotor, C is the axial external damping, M is the rotor mass, R is the phase winding resistance, L_c is the armature winding cyclic inductance, K_Φ is the flux gradient, i.e. the proportionality factor between the amplitude of the flux linkage due to the PMs and the axial position and k_e is the external axial stiffness. The latter could, for example, be related to detent effects or to the

axial stiffness induced by centering PM bearings. Hence, this stiffness is generally negative, as it is assumed hereafter.

Assuming quasi-static conditions, i.e. $\dot{z} = 0$, the electrodynamic axial stiffness $k(\omega)$ as well as the associated braking torque $T(\omega)$ can be retrieved from (1), yielding [17]:

$$k(\omega) = -\frac{F(\omega)}{z} = \frac{K_\Phi^2 N}{2L_c} \frac{\omega^2}{\omega^2 + \left(R/pL_c\right)^2}, \tag{3}$$

$$T(\omega) = -z^2 \frac{K_\Phi^2 N}{2L_c} \frac{R}{L_c} \frac{\omega}{\omega^2 + \left(R/pL_c\right)^2}. \tag{4}$$

As depicted in Fig. 2, illustrating the evolution of the stiffness, the latter increases with the spin speed and can be characterised through two coefficients, namely the rotor spin speed ω_e related to the electrical pole R/L_c and the asymptotic stiffness k_∞, defined as:

$$k_\infty = \frac{K_\Phi^2 N}{2L_c}. \tag{5}$$

Let us point out that the latter stiffness appears explicitly in the state matrix **A**, given in (2). On the contrary, as shown in Fig. 2, the braking torque $T(\omega)$ reaches its maximal value when the speed is equal to ω_e and then decreases asymptotically to zero.

IV. Stability Analysis

The behaviour of EDTBs is strongly dependent on the rotor spin speed and so is their stability. Hereinafter, general considerations about the stability of an EDTB coupled to the rotor are first derived. On this basis, the static and dynamic stability are then analysed, leading to conditions ensuring a stable behaviour at a specific rotor spin speed.

The following developments can be greatly simplified by considering the electrical pole as being much greater than the maximal natural frequency of the equivalent spring-mass system constituted of the rotor and the EDTB:

$$\frac{R}{L_c} \gg \sqrt{\frac{k_\infty}{M}}. \tag{6}$$

In this way, the electrical phenomena are much faster than the mechanical ones and thus do not have a significant impact on the rotor axial dynamics. Observing that the model given in (1) depends on the stiffness as well as the rotor mass and not their square roots, (6) can be expressed in a more convenient way as:

$$\left(\frac{R}{L_c}\right)^2 \gg \frac{k_\infty}{M}. \tag{7}$$

To the authors' best knowledge, the latter hypothesis is verified in the vast majority of the experimental and numerical studies of EDTBs, including the case study in section VI. In addition, let us assume a priori that the external damping satisfies:

$$2\left(\frac{C}{M}\right) \ll \frac{R}{L_c}. \tag{8}$$

This assumption will be verified a posteriori in section IV-C.

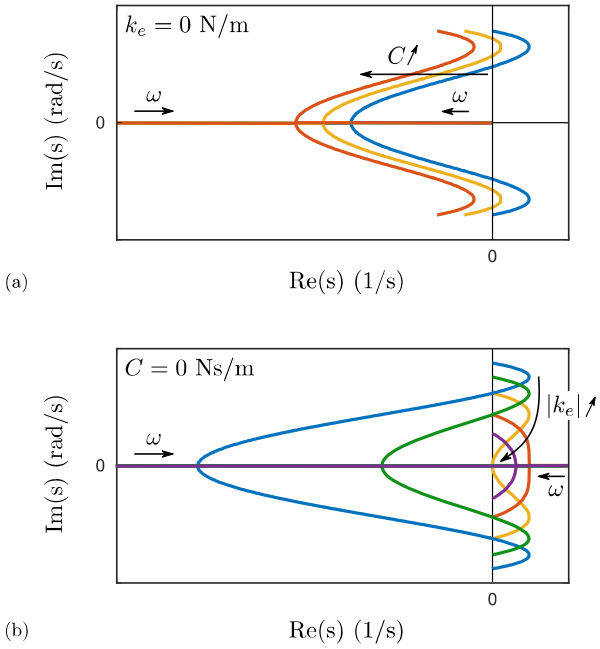

Figure 3. Evolution Root locus of both relevant eigenvalues. (a) Evolution with the damping C = {0; 0.5; 1} Ns/m for k_e = 0 N/m. (b) Evolution with the external stiffness k_e = {0; 0.25; 0.5; 0.75; 0.9} k_∞ N/m for C = 0 Ns/m.

A. General Considerations

The model in (1) being linear, the stability analysis can be performed through the study of the real part of the four eigenvalues of the state matrix **A** as a function of the spin speed. To this end, the characteristic polynomial is derived, and, under the hypothesis expressed in (7) and assuming (8) as verified, can be simplified as follows:

$$P(s) = s^4 + s^3\left(\frac{2R}{L_c}\right) + s^2\left(\frac{R^2}{L_c^2} + (\omega p)^2\right) + s\left(\frac{C}{M}\frac{R^2}{L_c^2}\right. \tag{9}$$
$$\left. + \frac{C}{M}(\omega p)^2 + \frac{R}{L_c}\frac{k_\infty + 2k_e}{M}\right) + \left(\frac{R^2}{L_c^2}\frac{k_e}{M} + \frac{k_\infty + k_e}{M}(\omega p)^2\right).$$

The root locus of the four eigenvalues can thus be obtained by finding the roots of (9) for different speeds. However, when it comes to stability analyses, only the speeds at which these eigenvalues cross the imaginary axis are relevant as they define the spin speed ranges within which the bearing is stable. Figs. 3(a) and 3(b) illustrate respectively the impact of the external damping and stiffness on the root locus. Only the two relevant eigenvalues, related to the mechanical behaviour, are represented, the remaining two, related to the electrical behaviour, being located far in the left half plane. The additional damping allows us to shift the complex conjugates parts of the root locus to the left by an amount equal to $C/(2M)$ whereas the external stiffness strongly modifies their shape.

As a result, there are at most three speeds ω_1, ω_2 and ω_3, defined in Fig. 4, corresponding to intersections with the imaginary axis. More precisely, as shown in Fig. 3, when the external damping approaches zero, the spin speed ω_3 tends to infinity and therefore no longer exists. By contrast, increasing the damping allows us to move the spin speeds ω_2 and ω_3 towards each other until they are equal, when the damping

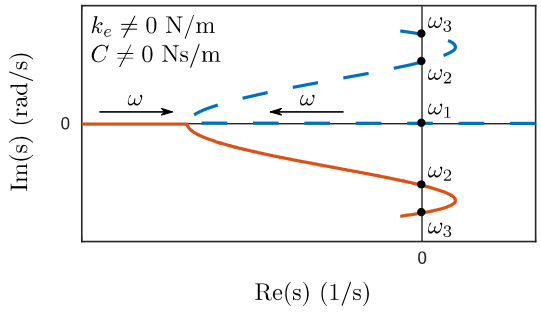

Figure 4. Root locus: spin speeds corresponding to intersections with the imaginary axis.

reaches a specific value, denoted by C_m hereinafter. Beyond the latter damping, these two speeds do not exist anymore. Besides, as illustrated in Fig. 3(b), the presence of the speed ω_2 strongly depends on the external stiffness.

For determining theses speeds, let us assume that $s = \mathrm{j}h$ implying that the eigenvalue lies on the imaginary axis. In this case, (9) can be separated into real and imaginary parts as follows:

$$\begin{cases} 0 = h^4 + \omega^2 p^2 \dfrac{k_\infty + k_e}{M} + \dfrac{R^2}{L_c^2}\dfrac{k_e}{M} - h^2\left(\dfrac{R^2}{L_c^2} + \omega^2 p^2\right) & (10) \\ 0 = h\left(\dfrac{C}{M}\left[\dfrac{R^2}{L_c^2} + \omega^2 p^2\right] + \dfrac{R}{L_c}\dfrac{k_\infty + 2k_e}{M}\right) - 2h^3\dfrac{R}{L_c}. & (11) \end{cases}$$

Solving (11) for h yields three solutions. As demonstrated hereinafter, one solution is related to a static instability whereas both remaining are linked to a dynamic one.

B. Static stability

The trivial solution of (11), i.e. $h = 0$, corresponds to the first intersection of the eigenvalues with the imaginary axis. Substituting this solution into (10) and isolating ω leads to:

$$\omega_1 = \frac{1}{p}\frac{R}{L_c}\sqrt{-\frac{k_e}{k_e + k_\infty}}. \quad (12)$$

This corresponds to the speed at which the stiffness induced by the electrodynamic effects compensates for the external stiffness, i.e. $k(\omega_1) = |k_e|$. Below this specific speed, the thrust bearing suffers from a static instability as the external stiffness, whose effect is destabilising due to its negative value, is larger than the electrodynamic one. This instability can be qualified as static as it does not depend on the damping. The static stability condition can thus be stated as:

$$k(\omega) \geq |k_e| \Leftrightarrow \omega \geq \omega_1. \quad (13)$$

Two limiting cases can be studied. On the one hand, when there is no external stiffness, the speed ω_1 is equal to zero and the static stability condition does not introduce any restriction on the rotor spin speed. On the other hand, when the external stiffness is larger, in absolute value, than the maximal electrodynamic stiffness, i.e. $|k_e| > k_\infty$, the speed ω_1 tends to infinity and the bearing is unstable regardless of the rotor spin speed.

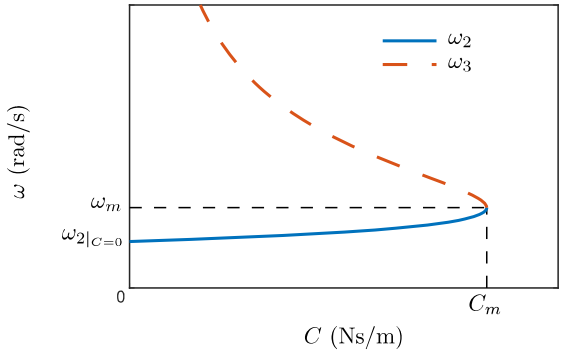

Figure 5. Evolution of the speeds ω_2 and ω_3 with the external damping C.

C. Dynamic stability

Both remaining solutions of (11) are linked to a dynamic instability as they depend on the damping. They can be calculated as follows:

$$h = \pm\sqrt{\frac{1}{2M}\left(\frac{R}{L_c}C + \frac{L_c}{R}C\omega^2 p^2 + k_\infty + 2k_e\right)}. \quad (14)$$

Substituting (14) into (10) and multiplying by $4R^2/L_c^2$ yields:

$$\omega^4 f_1 + \omega^2 f_2 + f_3 = 0. \quad (15)$$

The polynomial in (15) has at most two positive roots, thereby confirming that both eigenvalues related to the electrical behaviour never cross the imaginary axis. Under the hypothesis expressed in (7) and still assuming that the damping satisfies (8), the coefficients can be greatly simplified, leading to:

$$f_1 = -2p^4\frac{C}{M}\frac{R}{L_c}, \quad (16)$$

$$f_2 = 2p^2\left(\frac{R}{L_c}\right)^2\left[\frac{k_\infty}{M} - 2\frac{C}{M}\frac{R}{L_c}\right], \quad (17)$$

$$f_3 = -2\left(\frac{R}{L_c}\right)^4\left[\frac{k_\infty}{M} + \frac{C}{M}\frac{R}{L_c}\right]. \quad (18)$$

Solving (15) with these reduced coefficients allows us to determine both spin speeds ω_2 and ω_3 at which the relevant eigenvalues cross the imaginary axis, as shown in Fig. 4:

$$\omega_{2,3} = \frac{1}{p}\sqrt{\frac{1}{2}\frac{R}{L_c}\frac{M}{C}\left[\frac{k_\infty}{M} - 2\frac{C}{M}\frac{R}{L_c} \mp \sqrt{\left(\frac{k_\infty}{M}\right)^2 - 8\frac{R}{L_c}\frac{C}{M}\frac{k_\infty}{M}}\right]} \quad (19)$$

The value of these speeds is independent from the external stiffness k_e, signifying that the intersections of the eigenvalues with the imaginary axis occur at the same speeds even when the shape of the root locus is modified by the external stiffness. By contrast, as mentioned in section IV-A, the existence of these intersections strongly depends on the external damping and the external stiffness.

Fig. 5 shows the evolution of both speeds ω_2 and ω_3 with the external damping. As expected, when the latter is equal to zero, the speed ω_3 tends to infinity and therefore no longer exists whereas the speed ω_2 can be easily calculated by

observing that the coefficient f_1 in (16) is equal to zero, implying that (15) has only one positive solution:

$$\omega_2|_{C=0} = \frac{1}{p}\frac{R}{L_c} = \omega_e. \tag{20}$$

This speed thus corresponds to the spin speed ω_e related to the electrical pole. Let us point out that spin speeds smaller than this particular speed can never lie on the imaginary axis and are therefore stable, from a dynamic point of view, regardless of the damping. As stated in section IV-A, adding external damping enables to move the speeds ω_2 and ω_3 towards each other until they merge, when the damping reaches C_m. Cancelling the last term in (19) allows us to determine the value of this damping and the corresponding speed, denoted by ω_m:

$$C_m = \frac{k_\infty}{8}\frac{L_c}{R}, \qquad \omega_m = \frac{\sqrt{3}}{p}\frac{R}{L_c}. \tag{21}$$

Below this damping, the speeds ω_2 and ω_3 are distinct and the EDTB is unstable, from a dynamic point of view, when the speed belongs to the interval $[\omega_2\,;\omega_3]$, as shown in Fig. 4. By contrast, when the damping is larger than C_m, the eigenvalues only cross the imaginary axis at the speed ω_1 and the EDTB is stable beyond this speed. Consequently, unlike their static counterparts, dynamic instabilities can be removed through additional non-rotating damping.

Finally, substituting the maximal damping (21) into (8) and considering that the assumption in (7) is verified allows us to validate the relation (8) a posteriori, thus highlighting that the latter is not, as such, a hypothesis.

D. Stability conditions

In summary, the stability can be analysed on the basis of:

- the speed ω_1 related to the static instability, given in (12);
- the speeds ω_2 and ω_3, related to the dynamic instability, as a function of the damping, defined in (19);
- the external damping C added to the system.

More precisely, when the maximal electrodynamic stiffness is larger than the external one, i.e. $k_\infty > |k_e|$, the stability is ensured at the spin speed ω provided that:

$$\begin{cases} \omega \le \omega_2(C) \text{ or } \omega \ge \omega_3(C) & \text{if } C \in [0\,;C_m] \\ \omega \ge \omega_1. \end{cases} \tag{22}$$

Finally, let us point out that the state-space representations in [18][19] yield an identical characteristic polynomial, thus widening the scope of the previous developments to these electromechanical models.

V. Comparison Criteria

The stiffness, the losses and the stability are of primary interest when analysing a bearing. On this basis, four criteria can be derived to evaluate the intrinsic qualities of EDTB topologies, thus allowing us to compare them objectively. These criteria are independent from the rotor spin speed as well as its axial displacement.

A. Total Stiffness

In quasi-static conditions, the total stiffness $k_t(\omega)$, comprising both electrodynamic and external effects, can be expressed as:

$$k_t(\omega) = -\frac{F_t(z,\omega)}{z} = k(\omega) + k_e. \tag{23}$$

As stated above, the static stability of the system as well as the rotor axial position and dynamics are directly related to this stiffness. The maximal total stiffness $k_{t,\infty}$ therefore constitutes a first comparison criterion to be maximised:

$$k_{t,\infty} = k_\infty + k_e. \tag{24}$$

Further noting that, for fixed maximal stiffness $k_{t,\infty}$ and speed ω, decreasing the spin speed ω_e corresponding to the electrical pole allows us to increase the stiffness, the latter speed is a second criterion to be minimised:

$$\omega_e = \frac{1}{p}\frac{R}{L_c}. \tag{25}$$

B. Stability Margin

As stated above, adding non-rotating damping allows us to enlarge the range within which the system is stable. However, to be coherent with the magnetic bearing approach, the external damping should be contactless. Considering the potential difficulty of producing the latter, the damping required to stabilise the thrust bearing regardless of the spin speed, namely C_m defined in (21), should be minimised. This is all the more true observing that maximising the stiffness and thus minimising the speed ω_e corresponding to the electrical pole reduces the stable speed range when there is no external damping.

C. Energy efficiency coefficient

In addition to the restoring force, the thrust bearing produces an electrodynamic braking torque, therefore contributing to decrease the rotor spin speed. The power P related to this braking torque is entirely dissipated in the winding resistances in the form of Joule losses, leading to a rise in temperature and thus being potentially detrimental to the functioning of the bearing. In quasi-static conditions, these rotational losses can be calculated as:

$$P(\omega) = |\omega\, T(\omega)| = z^2 k_\infty \frac{R}{L_c}\frac{\omega^2}{\omega^2 + \left({}^{R}/_{pL_c}\right)^2}. \tag{26}$$

The bearing purpose is to provide the largest axial levitation force F_t whereas the associated rotational losses P have to be minimised. This amounts to maximising the following ratio:

$$\frac{F_t}{\sqrt{P}} = \sqrt{\frac{(k_\infty + k_e)^2}{k_\infty}\frac{L_c}{R}\frac{[(p\omega)^2 - (p\omega_1)^2]^2}{(p\omega)^2\left[(p\omega)^2 + \left(\frac{R}{L_c}\right)^2\right]}}. \tag{27}$$

This ratio therefore only exists for rotor spin speeds larger than ω_1, increasing from zero up to reach its asymptotic value denoted by K_p:

$$K_p = \sqrt{\frac{(k_\infty + k_e)^2}{k_\infty}\frac{L_c}{R}}. \quad (28)$$

The energy efficiency coefficient K_p thus constitutes a fourth comparison criterion to be maximised. Lastly, in the absence of external stiffness, (28) reduces to:

$$K_p\big|_{k_e=0} = \sqrt{k_\infty \frac{L_c}{R}}. \quad (29)$$

The latter coefficient is proportional to the square root of the external damping C_m required to stabilise the bearing regardless of the spin speed, given in (21). However, the energy efficiency has to be maximised whereas the additional damping has to be minimised. A trade-off between these two criteria must therefore be considered, depending in particular on the application requirements as regards losses and spin speed.

VI. Case Study

The case study is performed on the three EDTBs illustrated in Fig. 6. The first corresponds to a topology with a merged armature winding as internal subassembly and is denominated topology 1. The second bearing, denominated topology 2, corresponds to the topology with two distinct PM arrangements as internal subassembly and the armature winding consisting of two sets of p coils connected in series, the two resulting sets being themselves connected in opposition. The last one, denominated topology 3, is identical to the second but includes in addition back irons on which the sets of coils are placed. In each of these topologies, the PM arrangements comprise ferromagnetic yokes, the remanent magnetisation is 1.42 T and the number p of pole pairs is two. The armature winding comprises three phases ($N = 3$) and the conductor density, defined as the number of conductors per unit of coil section, is 4/mm^2. The rotor includes the armature winding and its mass is set to 1 kg. Lastly, the overall dimensions of the topologies, given in Table I, are identical and so is their PM volume.

TABLE I. Study case: bearing dimensions (mm)

R_i	R_o	h_y	h_{PM}	e	t_w	l	h_b	h_w
10	50	2	3	3	5	10	2	parameter

A. Parametric Analysis

For each topology, a parametric analysis of the four comparison criteria defined above is performed with respect to the winding thickness h_w. To this end, the model parameters are identified for all configurations through static finite element simulations by applying the methods detailed in [17]. As illustrated in Fig. 7(a), the square of the ratio between the natural frequency of the equivalent spring-mass system and the electrical pole stays below 7%, therefore validating the assumption in (7) as well as the resulting developments with regard to the stability analyses and the external damping required to stabilise the bearing.

Fig. 7(b) shows the evolution of the maximal total stiffness with the winding thickness. The first topology reaches its maximum, namely 25.5 N/mm, when the thickness is equal to 10 mm whereas the second one has a peak value of 23.5 N/mm

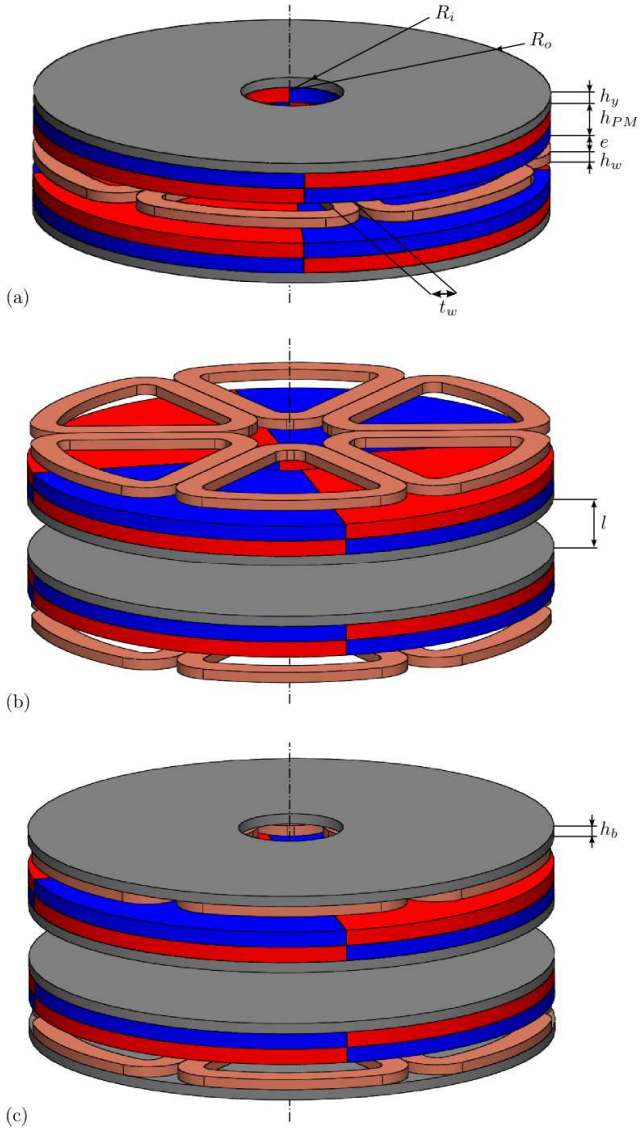

Figure 6. Study case: bearing topologies. (a) Topology 1. (b) Topologies 2. (c) Topology 3.

for a thickness of 2 mm. Furthermore, below a thickness of about 6.2 mm, represented by a dotted line, the total stiffness of the third topology is negative, meaning that the detent force due to the interaction between the PMs and the back irons is larger than the electrodynamic one and thus leading to a static instability regardless of the speed. Above this particular thickness, the total stiffness increases until it joins the curve related to the second topology without ever exceeding the latter. The presence of the back irons is therefore clearly not attractive as regards axial stiffness.

Fig. 7(c) shows the evolution of the spin speed ω_e corresponding to the electrical pole with the winding thickness. Regardless of the latter, the first topology shows smaller speeds ω_e than the second one, signifying that the stiffness reaches its maximum at lower speeds. However, the discrepancy between these two topologies decreases with the thickness. As regards the third topology, as soon as the total

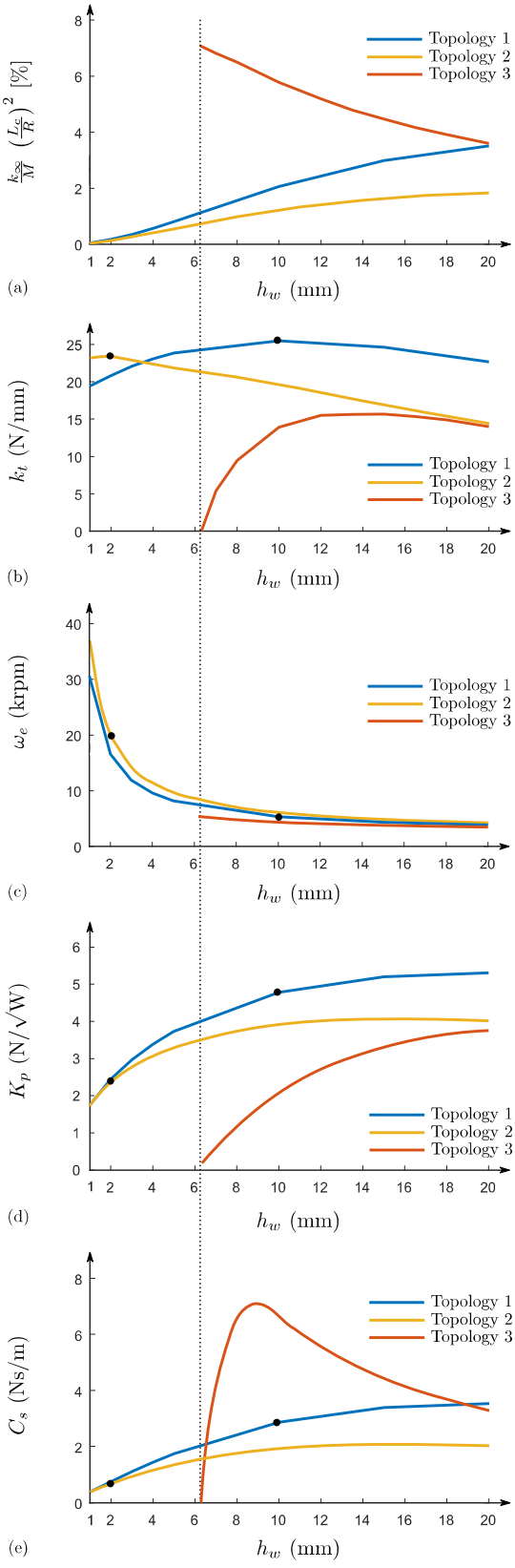

Figure 7. Study case: evolution of the comparison criteria with the winding thickness for the three topologies. (a) Hypothesis validation. (b) Maximal total stiffness. (c) Spin speed related to the electrical pole. (d) Energy efficiency coefficient. (e) Stability margin.

stiffness becomes positive, the electrical pole remains smaller than the one related to the second topology given that the back irons allows us to increase the cyclic inductance while maintaining the resistance unchanged.

Fig. 7(d) shows the evolution of the energy efficiency coefficient K_p with the thickness. As regards this criterion, the topologies 1 and 2 are rather close for small thicknesses. However, the former always outclasses the latter and the gap widens with the winding thickness. In comparison with these two topologies, the efficiency of the third one remains quite low due to the negative contribution of the detent force.

Fig. 7(e) shows the evolution of the damping required to stabilise the bearing at high speeds with the winding thickness. As mentioned in section V-C, the damping related to the topologies 1 and 2 presents an identical shape to the curves linked to the energy efficiency, given that the latter is proportional to the square root of the required damping in the absence of external stiffness. More precisely, it remains limited to relatively small values, namely no more than 2.0 and 3.5 Ns/m respectively. By contrast, the third topology requires slightly larger damping with up to the double, i.e. 7.2 Ns/m.

In summary, the first topology is attractive for a winding thickness close to 10 mm as the stiffness k_∞ is maximal whereas the spin speed related to the electrical pole is rather low, namely 5200 rpm. Besides, the energy efficiency coefficient is important and the required damping, being equal to 2.9 Ns/m, can be considered as reasonable in light of the values reported in the literature [21]. The second topology with a winding thickness equal to 2 mm yields an almost equivalent maximal stiffness although the electrical pole is about four times larger. The required damping is thus smaller for this topology, being equal to 0.71 Ns/m, and therefore easier to produce. However, it also means that the energy efficiency is reduced by a factor about 2. Let us point out that, without considering the distance l between both parts of the second topology, the volume occupied by both topologies is nearly identical. Only the first and second topologies with a winding thickness equal to 10 and 2 mm respectively are considered hereinafter.

B. *Stiffness Analysis*

Let us study the evolution of the stiffness with the rotor spin speed for the topologies 1 and 2. Figs. 8(a) and 8(b) represent respectively, while taking into account the stability conditions for each spin speed and amount of external damping, the maximal stiffness among both topologies and the corresponding topology. The solid and dashed lines illustrate the evolution of the speed ω_2 and ω_3 with the damping for the first and second topology respectively, thereby forming their respective stability boundaries. Indeed, below each curve, the corresponding topology suffers from a dynamic instability. Consequently, both topologies are unstable in the white zone.

Regardless of the spin speed, the topology 1 provides a higher stiffness and reaches its maximal stiffness k_∞ for lower speeds than the topology 2 given that the electrical pole is smaller. By contrast, in the absence of additional damping, the topology 1 is also unstable from a smaller speed. Indeed, as stated in section V-A, minimising the spin speed ω_e related to

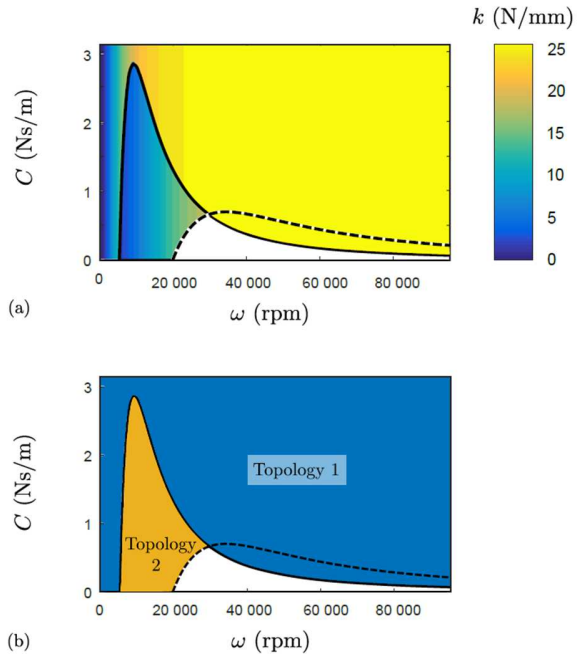

Figure 8. Study case: comparison of the stiffness of topologies 1 and 2 while taking into account their stability boundaries (solid and dashed lines respectively). (a) Maximal stiffness with the spin speed. (b) Corresponding topology.

the electrical pole amounts to reducing the stable speed range when there is no external damping. Therefore, between about 5000 and 20 000 rpm, namely the spin speeds related to the electrical poles of both topologies, the second one offers the major advantage of not requiring external damping to ensure the axial stable levitation of the rotor. This brief analysis underlines that the rotor spin speed can still strongly influence the bearing selection according to the application specifications.

VII. Conclusions

This paper presents four criteria allowing us to compare objectively various electrodynamic thrust bearing topologies based on their intrinsic qualities and therefore to determine the most appropriate.

On the basis of the recent linear state-space representations describing the axial dynamics of EDTBs, an analytical static and dynamic stability analysis is performed through the calculation of the eigenvalues of the state matrix. The impact of the external damping and external stiffness is studied through a root locus as a function of the rotor spin speed, highlighting that the former allows us to move the eigenvalues to the left, thus improving the stability, whereas the latter modifies their shape. Besides, the spin speeds corresponding to intersections with the imaginary axis are calculated, therefore defining the ranges within which the thrust bearing is stable. In the absence of additional damping and external stiffness, the thrust bearing is stable up to the spin speed related to the electrical pole.

When it comes to comparing magnetic bearings, the maximal eccentricity, the losses and the stability are of primary interest. As a result, the four following comparison criteria are defined: (i) the maximal total stiffness, (ii) the spin speed corresponding to the electrical pole, (iii) the levitation energy efficiency, defined as the ratio between the thrust force and the square root of the corresponding rotational losses, and (iiii) the damping required to stabilise the bearing regardless of the rotor spin speed. Three different thrust bearing topologies, studied in the framework of a case study, are finally compared on the basis on these criteria, notably highlighting that the addition of back irons behind the sets of coils has no beneficial effect as regards axial dynamics due to the important detent stiffness.

Future research prospects include the exploitation of these comparison criteria in a process of optimal design of an EDTB.

Acknowledgements

J. Van Verdeghem is a FRIA Grant Holder of the Fonds de la Recherche Scientifique-FNRS, Belgium.

References

[1] G. Schweitzer and E. Maslen, Magnetic Bearings: Theory, Design, and Application to Rotating Machinery. Berlin: Springer-Verlag, 2009.

[2] R. F. Post, “Stability issues in ambient-temperature passive magnetic bearing systems,” NASA STI/Recon Technical Report N, vol. 3, 2000.

[3] A. V. Filatov and E. H. Maslen, “Passive magnetic bearing for flywheel energy storage systems,” IEEE Transactions on Magnetics, vol. 37, no. 6, pp. 3913–3924, Nov 2001.

[4] J. G. Detoni, F. Impinna, A. Tonoli, and N. Amati, “Unified modelling of passive homopolar and heteropolar electrodynamic bearings,” Journal of Sound and Vibration, vol. 331, no. 19, pp. 4219 – 4232, 2012.

[5] C. Dumont, V. Kluyskens, and B. Dehez, “Linear state-space representation of heteropolar electrodynamic bearings with radial magnetic field,” IEEE Transactions on Magnetics, vol. 52, no. 1, pp. 1–9, Jan 2016.

[6] N. Amati, X. D. Lepine, and A. Tonoli, “Modeling of electrodynamic bearings,” Journal of Vibration and Acoustics, vol. 130(6), 2008.

[7] N. Amati, A. Tonoli, E. Zenerino, J. G. Detoni, and F. Impinna, “Design methodology of electrodynamic bearings,” in Proceedings of the XXXVIII National Meeting of the Italian Society of Mechanical Engineers (AIAS), Torino, Italy, 2009.

[8] C. Dumont, V. Kluyskens, and B. Dehez, “Yokeless radial electrodynamic bearing,” Mathematics and Computers in Simulation, vol. 130, pp. 57 – 69, 2016, 11th International Conference on Modeling and Simulation of Electric Machines, Converters and Systems.

[9] C. Dumont, V. Kluyskens, and B. Dehez, “Impact of the yoke material on the performance of wounded electrodynamic bearings,” in International Symposium on Magnetic Bearings, Linz, Austria, 2014.

[10] P. Basore, “Passive stabilization of flywheel magnetic bearings,” MIT Master Thesis, 1978.

[11] A. Filatov, “Null-e magnetic bearings,” Ph.D. dissertation, 2002.

[12] J. G. Detoni, F. Impinna, N. Amati, and A. Tonoli, “Rotational power loss on a rotor radially supported by electrodynamic passive magnetic bearings,” in Proc. of the 5th world tribology congress, 2013, pp. 1–4.

[13] V. Kluyskens and B. Dehez, “Dynamical electromechanical model for magnetic bearings subject to eddy currents,” IEEE Transactions on Magnetics, vol. 49, no. 4, pp. 1444–1452, April 2013.

[14] A. Tonoli, N. Amati, F. Impinna, and J. G. Detoni, “A solution for the stabilization of electrodynamic bearings: Modeling and experimental validation,” Journal of Vibration and Acoustics, vol. 133, no. 2, p. 021004, 2011.

[15] K. Davey, A. Filatov, and R. Thompson, “Design and analysis of passive homopolar flux bearings,” IEEE Transactions on Magnetics, vol. 41, no. 3, pp. 1169–1175, March 2005.

[16] M. E. Storm, “The application of electrodynamic levitation in magnetic bearings,” Ph.D. dissertation, North-West University, 2006.

[17] J. Van Verdeghem, C. Dumont, V. Kluyskens, and B. Dehez, “Linear state-space representation of the axial dynamics of electrodynamic thrust

bearings," IEEE Transactions on Magnetics, vol. 52, no. 10, pp. 1–12, Oct 2016.

[18] F. Impinna, J. G. Detoni, N. Amati, and A. Tonoli, "Passive magnetic levitation of rotors on axial electrodynamic bearings," IEEE Transactions on Magnetics, vol. 49, no. 1, pp. 599–608, Jan 2013.

[19] N. Amati, J. Detoni, F. Impinna, and A. Tonoli, "Axial and radial dynamics of rotors on electrodynamic bearings," in 10th International Conference on Vibrations in Rotating Machinery, IMechE, Ed. Woodhead Publishing, 2012, pp. 113 – 122.

[20] J. Van Verdeghem, V. Kluyskens, and B. Dehez, "Five degrees of freedom linear state-space representation of electrodynamic thrust bearings," Journal of Sound and Vibration, vol. 405, pp. 48 – 67, 2017.

[21] B. Ebrahimi, M. B. Khamesee, and F. Golnaraghi, "Permanent magnet configuration in design of an eddy current damper," Microsystem Technologies, vol. 16, no. 1, p. 19, Nov 2008.